

Cavity phenomena in mesas of cuprate high- T_c superconductors under voltage bias

Xiao Hu^{1,2,3} and Shizeng Lin^{1,2}

¹WPI Center for Materials Nanoarchitectonics, National Institute for Materials Science, Tsukuba 305-0044, Japan

²Graduate School of Pure and Applied Sciences, University of Tsukuba, Tsukuba 305-8571, Japan

³Japan Science and Technology Agency, 4-1-8 Honcho, Kawaguchi, Saitama 332-0012, Japan

(Dated: November 2, 2018)

Modeling a single crystal of cuprate high- T_c superconductor, such as $\text{Bi}_2\text{Sr}_2\text{CaCu}_2\text{O}_{8+\delta}$, as a stack of intrinsic Josephson junctions, we formulate explicitly the cavity phenomenon of plasma oscillations and electromagnetic (EM) waves in mesas of cylindrical and annular shapes. When the mesa thickness is small compared with the EM wavelength, the boundary condition for the inductively coupled sine-Gordon equations is the Neumann-type one to a good approximation, addressed first theoretically and verified in a recent experiment. This renders the superconductor mesa a cavity. Biasing a dc voltage in the c direction, a state with $\pm\pi$ kinks in the superconductivity phase difference piled up alternatively along the c axis is stabilized. The $\pm\pi$ phase kinks provide inter-lock between superconductivity phases in adjacent junctions, taking the advantage of huge inductive couplings inherent in the cuprate superconductors, which establishes the coherence across the whole system of more than ~ 600 junctions. They also permit a strong coupling between the lateral cavity mode and the transverse Josephson plasma, enhance the plasma oscillation significantly at the cavity modes which radiates EM waves in the terahertz band when the lateral size of mesa is set to tens of micrometers. In order to overcome the heating effect, we propose to use annular geometry. The dependence of frequency on the aspect ratio is analyzed, which reveals that the shape tailor is quite promising for improving the present technique of terahertz excitation. The annular geometry may be developed as a waveguide resonator, mimic the fiber lasers for visible lights.

PACS numbers: 74.50.+r, 74.25.Gz, 85.25.Cp

I. INTRODUCTION

The Josephson effect provides a unique principle to excite high-frequency electromagnetic (EM) waves [1, 2]. Much effort has been made to stimulate powerful radiations, first using artificial Josephson junction arrays [3, 4, 5, 6, 7, 8, 9, 10], and later on Josephson junctions inherent in cuprate high- T_c superconductors of layered structures [11, 12, 13, 14, 15, 16, 17, 18, 19, 20, 21, 22, 23, 24, 25]. The latter have obvious advantages, since the junctions are homogeneous at the atomic scale guaranteed by the high quality of single crystals, and the superconductivity gap is large, typically of tens of meV, which in principle permits the frequency cover the whole range of the terahertz (THz) band, a very useful regime of EM waves still lacking of compact solid-state generators [26, 27].

An experimental breakthrough was achieved in 2007 [28]. Clear evidences have been obtained that coherent terahertz radiations from side edges of a thin rectangular mesa were realized by biasing a dc voltage in the c axis of the $\text{Bi}_2\text{Sr}_2\text{CaCu}_2\text{O}_{8+\delta}$ (BSCCO) single crystal; the frequency of the EM wave and the voltage where the radiation occurs obey the ac Josephson relation, and the frequency coincides with one of the cavity modes determined by the lateral size of mesa [28].

This discovery is expected to leave significant and long-standing impacts. It has the potential to open a practical way to develop a source of frequency tunable EM waves based on superconductivity and fill the so-called THz-gap. It also shines light on new directions of making use of the phase of superconductivity. Its importance would

be better appreciated if one notices that up to now the usage of superconductivity phase variable is still limited to the SQUID.

The discovery immediately raises many interesting questions, such as why the Josephson plasma oscillation, namely the coherent tunneling of Cooper pairs forth and back between adjacent CuO layers driven by a c -axis voltage can radiate strong *transverse* radiations, in absence of Josephson vortices induced by an applied magnetic field; how it becomes possible to synchronize the superconductivity phase variables of ~ 600 junctions, and so on. These quests challenge our knowledge on superconductivity as well as nonlinear phenomena.

It is formulated explicitly in Ref. [22] that there is a significant mismatch in impedance $|Z_{\text{out}}|/|Z_{\text{in}}| \sim \lambda_{\text{EM}}/L_z$ at the edge of a superconductor mesa when the thickness of the mesa L_z is small compared with the EM wavelength λ_{EM} , which was known for a single junction as a limiting case [29]. This makes the tangential component of oscillating magnetic field at the mesa edge extremely small compared with the electric one, in sharp contrast to the case of EM plane waves. Actually, this relation is a general property shared by a normal capacitor with small electrode separation. Particularly for thin mesas of superconductor, the vanishingly small tangential component of magnetic field gives the Neumann-type boundary condition of superconductivity phase difference across junctions, namely the spatial derivative of the phase difference normal to the edge should be zero (in absence of an applied magnetic field).

With this Neumann boundary condition, a new dynamic state of superconductivity phase difference has

been found in a stack of Josephson junctions under a dc voltage bias, which is characterized by static $\pm\pi$ (actually $\pm(2m+1)\pi$ with m integer) phase kinks localized at the mesa center and piled up alternatively along the c axis [30, 31, 32, 33]. In this π kink state, an inter-lock between superconductivity phases in neighboring junctions appears, which establishes the coherence across the whole system of more than ~ 600 junctions. The π phase kink makes the lateral cavity modes and the transverse Josephson plasma couple strongly to each other, permits large dc supercurrent flow into the junctions and generates strong EM radiations from the sides of mesa.

The π kink state requests strong inductive couplings between adjacent superconducting layers [30], which is guaranteed in the cuprates high- T_c superconductor BSCCO. Another condition is on the thickness of the superconductor mesa: it should be much smaller than the EM wavelength on one hand, which renders the superconductor mesa a cavity, and on the other hand, it should be thick enough to avoid large surface effects. The samples of $L_z \simeq 1\mu\text{m}$ adopted in the experiment [28] satisfy these requests well. The π kink state is stable against other distortions, such as thermal fluctuations, inhomogeneity of physical parameters, and so on.

The present work is motivated by two recent experiments on THz radiations from thin mesas of BSCCO single crystals. The first one is a detection of THz radiations from a cylindrical mesa [34], after the theoretical proposal [31] for testifying the boundary condition of the system. The second one is an observation on EM standing waves in a rectangular mesa [35], an approach being able to provide direct evidence for cavity resonance.

The remaining part of the present paper is organized as follows. In Sec. II, we discuss the right boundary condition for thin mesas from a theoretical point of view. Then we point out that the result of the recent experiment using a cylindrical mesa is to be understood in accordance with this boundary condition. In Sec. III, the radius dependence of the radiation frequency for first several modes is presented, accompanied with the spatial distributions of the π kink in superconductivity phase difference, supercurrent, as well as the EM standing wave. Section IV is devoted to a new proposal of using annular mesa, which can reduce the Joule heating and enhance the leakage of heat as compared with the cylindrical one. By checking the frequency variation upon tuning aspect ratio, it is displayed that tailoring the mesa geometry may be a prosperous way to improve the present technique for THz stimulation. Finally summary and perspectives are given in Sec. V.

II. BOUNDARY CONDITION AND CYLINDRICAL MESA

A. Basic equation and general solution

The inductively coupled sine-Gordon equations for the gauge-invariant phase differences in a stack of Josephson junctions with a dc current bias and dissipations are given in the dimensionless form as [30, 31, 33]

$$\Delta P_l = (1 - \zeta\Delta^{(2)})(\sin P_l + \beta\partial_t P_l + \partial_t^2 P_l - J_{\text{ext}}), \quad (1)$$

under the Neumann boundary condition in the lateral directions $\partial_n P_l = 0$; $\zeta \equiv \lambda_{ab}^2/(s+D)^2 \sim 10^5$ is the inductive coupling and $\beta \equiv 4\pi\sigma_c\lambda_c/c\sqrt{\varepsilon} = 0.02$ is the c -axis conductivity; Δ the Laplace operator in lateral directions, and $\Delta^{(2)}Q_l = Q_{l+1} + Q_{l-1} - 2Q_l$ the second difference operator along the c axis. The lateral space is scaled by λ_c and time by $c/\lambda_c\sqrt{\varepsilon}$. For more details of definitions see Refs. [30, 31, 33].

The experimental observation of the cavity relation of radiation frequency [28, 36] indicates that standing waves of plasma oscillation has been built in the cavity formed by the mesa, which in turn implies that the oscillating part of the phase difference satisfies the Laplace equation [30, 31, 33]. The plasma oscillation should be uniform since the observed radiations are coherent, known as a superradiation [28]. Without losing generality, the solution to Eq. (1) can be given by

$$P_l(\mathbf{r}, t) = \omega t + \tilde{P}(\mathbf{r}, t) + f_l P^s(\mathbf{r}), \quad (2)$$

where the first term accounts for the finite dc bias voltage, and the second for plasma oscillation

$$\tilde{P}(\mathbf{r}, t) = Ag(\mathbf{r}) \sin(\omega t + \varphi) \quad (3)$$

with A the amplitude, $g(\mathbf{r})$ an eigenfunction of the Laplace equation with the Neumann boundary condition for the corresponding geometry, and the frequency given by the voltage following the ac Josephson relation; the third term carries the inter-junction coupling via the l dependence.

The general form of Eq. (2) describes a wealth of solutions even giving the constraint imposed by available experimental results. However, it is easy to see [30, 31, 33] that the sequences $f_l = (-1)^l$ or $f_l = (-1)^{\lfloor l/2 \rfloor}$ with period 2 or 4 layers respectively diagonalize Eq. (1) due to the property of the difference operator $\Delta^{(2)}$. In simulations, these two states appear frequently and are stable [30, 33]. Here we focus the attention to these two cases.

The static phase $P^s(\mathbf{r})$ should then satisfy the differential equation

$$\Delta P^s = q\zeta \cos \varphi J_1(Ag(\mathbf{r})) \sin P^s, \quad (4)$$

with the same boundary condition of the total phase difference, where $q = 4$ and 2 for the c -axis sequence of period 2 and 4 respectively.

The static phase factor $P^s(\mathbf{r})$, amplitude A , phase shift in plasma oscillation φ and total current J_{ext} can be solved for a given voltage (or equivalently ω) [30, 31]. The nontrivial solution $P^s(\mathbf{r})$ presumes the π phase kink [30, 31, 32, 33]. The static c -axis supercurrent which contributes to the net current flowing into the system in the c direction is given by

$$J_s(\mathbf{r}) = \sin \varphi J_1(Ag(\mathbf{r})) \cos(P^s(\mathbf{r})). \quad (5)$$

We point out that the claim in Ref. [37] on a very non-linear IV characteristics in the absence of π kinks is not compatible with Eq. (5) and needs further check.

The trivial vacua solution $P^s = 0$ is dropped here, which gives a linear IV and a broad voltage regime with weak radiations, inconsistent with experiments [28, 36]. See Ref. [33, 38] for more discussions on this vacua state.

It is noticed that only the fundamental frequency is taken in Eq. (3) since higher harmonics are small especially in cylindrical and annular geometry, where the higher harmonic frequencies appearing in the expansion of the sine function of the dc Josephson relation are not the cavity frequency.

The oscillating electric and magnetic fields inside the junctions are given by the plasma oscillation term of the phase difference in dimensionless forms as

$$E^z(\mathbf{r}, t) = \frac{\partial \tilde{P}}{\partial t}, \quad (6)$$

with $E^x, E^y \simeq 0$ to a good approximation in cuprates [30], and

$$\mathbf{B}(\mathbf{r}, t) = -\nabla \times (\tilde{P}(\mathbf{r}, t)\hat{\mathbf{z}}), \quad (7)$$

with $\hat{\mathbf{z}}$ the unit vector in the c axis. It is Eq. (7) that enforces the boundary condition for the phase difference $\partial_n P_l = 0$ with n the normal of the sample edges.

B. Testifying the boundary condition

In a rectangular mesa, the spatial part of the plasma term of the lowest cavity mode satisfying the right boundary condition is $\cos(x\pi/L)$. Unfortunately, $\cos(x\pi/L)$ and $\sin(x\pi/L)$ are both eigenfunctions of the Laplace equation, derivative to each other, and give the same wave number (or equivalently frequency in dimensionless form) π/L . Therefore, from a pure experimental point of view, the dependence of frequency on the system size cannot determine uniquely the mode.

A mesa of cylindrical shape was proposed to testify uniquely the dynamics of the superconductivity phase

difference inside the junctions [31]. For the cylinder geometry, the radial part of an eigenfunction of the Laplace equation is given by the Bessel function, not their derivatives. The boundary condition for the cylinder geometry determines uniquely the wave number, and vice versa, since the zeros of the Bessel functions are different from the zeros of their derivatives, contrasting to sine and cosine functions in the rectangle geometry. Therefore, measuring by experiments the frequency of EM radiation from a cylindrical mesa of given radius and assigning the mode by the properties of Bessel functions enable one to identify uniquely the right boundary condition for the EM waves. It was addressed that, from the boundary condition suitable for thin mesas, the frequency of radiation should be given by the zeros of derivatives of Bessel functions [31]. A case of the (0,1) mode, which is uniform azimuthally, has been worked out explicitly, and the frequency is figured out as $k_{01}^c = \chi_{01}^c/a$ with the radius a and $\chi_{01}^c = 3.8317$ the first zero of derivative of the Bessel function $J_0(z)$ [39].

The recent experiment [34] showed that the frequency of EM wave radiated from the cylindrical mesa of radius $a \simeq 45\mu\text{m}$ is $f \simeq 0.474\text{THz}$. With the light velocity in the sample $c' = c/\sqrt{\varepsilon} \simeq 7.16 \times 10^7\text{m/s}$ ($\varepsilon \simeq 17.54$ [40]), the wave number observed in the experiment [34] is given by $k \simeq 1.87/a$. Since $\chi = 1.8412$ is the first zero of derivative of the Bessel function $J_1(z)$, it is inferred that the mode (1,1) has been achieved in the experiment. The most important message from the experiment is that the frequency of EM radiation is determined by the zero of derivative of the Bessel function, in agreement with the theoretical analysis [31]. The right boundary condition for the cavity therefore is that the tangential component of the oscillating magnetic field should be zero at the edges as discussed above, consistent with the analysis in Ref. [22]. The (1,1) cavity mode for the cylinder geometry assumes a lower frequency than the (0,1) mode due to the positions of zeros of derivatives of Bessel functions [39], and thus is realized at a low voltage while the (0,1) mode might be difficult to excite in experiment where the heating effect is crucial.

III. MODES FOR CYLINDRICAL MESA

Knowing the right boundary condition, it is not hard to figure out the EM standing waves for all the cavity modes. Since their distribution can be observed directly in experiments [35] and serves as a check of the theory, we map them out explicitly. The distributions of superconductivity phase difference and the supercurrent are helpful for understanding the way how large dc powers are converted to high-frequency transverse radiations.

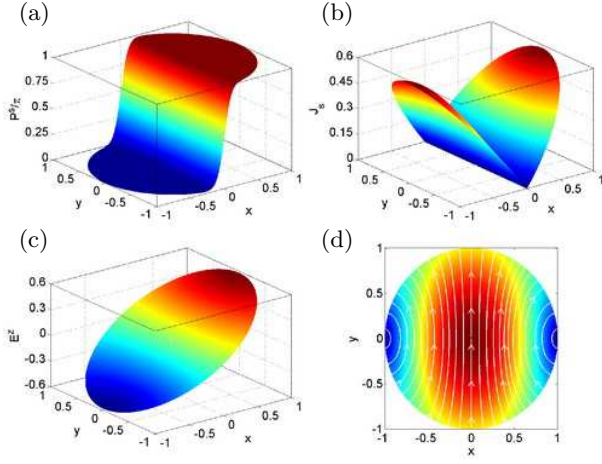


FIG. 1: (color online). Spatial distribution of (a) the static phase term P^s , (b) supercurrent, and the standing (c) electric and (d) magnetic wave for the (1,1) mode of a cylindrical mesa. Here $\zeta' = qA\zeta \sin \varphi = 5000$ is taken for Eq. (4) in (a) and the kink is approximated as a step function in (b) corresponding to $\zeta = \infty$. The lateral coordinates are normalized by the radius of the cylinder. The quantities except the phase difference P^s are up to the plasma amplitude A .

A. (1,1) mode for cylindrical mesa

All the modes (m, n) for the cylindrical geometry can be classified according to the number of symmetry axes in the azimuthal direction, m , and the number of maxima and minima along the radial direction, n , in the spatial part of plasma oscillation and electric field (see Eq. (6)), which all correspond to the zeroes of the derivative of Bessel functions. The solution to Eq. (1) assigned as the (1,1) mode for the cylinder geometry is given by

$$P_l(\mathbf{r}, t) = \omega t + AJ_1\left(\frac{\chi_{11}^c}{a}\rho\right) \cos \phi \sin(\omega t + \varphi) + f_l P^s(\mathbf{r}), \quad (8)$$

where the cylindrical coordinates are given by $\mathbf{r} = (\rho, \phi)$; $\chi_{11}^c = 1.8412$ is the first zero of the derivative of $J_1(z)$. For a cylinder with uniform physical properties, the eigenfunction for the azimuthal angle $\sin \phi$ degenerates with $\cos \phi$, which, and any linear combination of them, can be absorbed into the latter by redefining the azimuthal angle ϕ , and will not be discussed explicitly.

The wave number, and equivalently frequency ($k = f$ in dimensionless form and $k = c'f$ with units), of this mode is given by $k_{11}^c = \chi_{11}^c/a = 1.8412/a$, which agrees well with the experiment [34] as discussed in the previous section.

The distribution of the static phase P^s , supercurrent and the spatial part of the oscillating electric and magnetic fields are displayed in Fig. 1. The π phase kink runs along the diameter at the direction $\phi = \pm\pi/2$, and the phase difference saturates to 0 and π at the left and right part of the cylinder (Fig. 1(a)).

Associated with the static phase kink, the oscillating

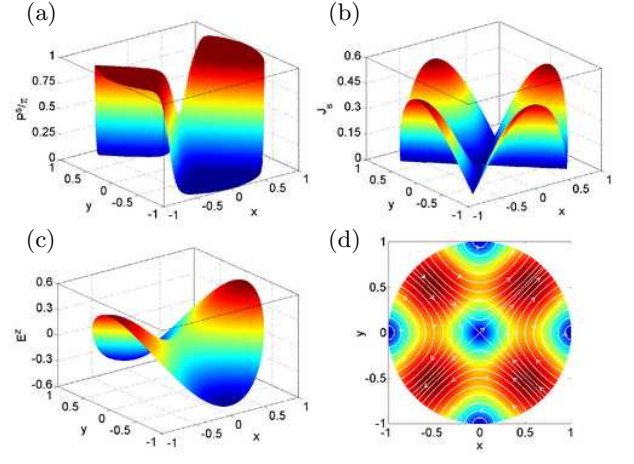


FIG. 2: (color online). Same as Fig. 1 for the (2,1) mode of a cylindrical mesa.

magnetic field assumes the maximal absolute value along the diameter at $\phi = \pm\pi/2$, and decreases to zero at the left- and right-most parts of the cylinder (Fig. 1(d)). The azimuthal component of the magnetic field is always zero at the edge of cylinder, as imposed by the boundary condition. The electric field takes its maximal absolute value at the left- and right-most parts, while is reduced to zero along the diameter at $\phi = \pm\pi/2$ (Fig. 1(c)).

Comparing the distributions of the π phase kink and the electric and magnetic field, it is found that the (1,1) mode for the cylinder geometry corresponds to the (1,0) mode for the rectangle geometry [31].

The maximal value of the supercurrent takes place at the left- and right-most part of the cylinder for the present mode. The factor $\cos(P^s(\mathbf{r}))$ from the π phase kink (Fig. 1(a)) renders the supercurrent associated with the cavity mode $J_1(Ag(\mathbf{r}))$ positive over the cylinder (Fig. 1(b)), which permits large bias current when the plasma amplitude A is enhanced at the cavity resonance.

B. (2,1) mode for cylindrical mesa

The (2,1) mode in the cylindrical mesa is given by

$$P_l(\mathbf{r}, t) = \omega t + AJ_2\left(\frac{\chi_{21}^c}{a}\rho\right) \cos(2\phi) \sin(\omega t + \varphi) + f_l P^s(\mathbf{r}), \quad (9)$$

with $\chi_{21}^c = 3.0542$ the first zero of the derivative of $J_2(z)$. The patterns for the (2,1) mode are displayed in Fig. 2. There are two pairs of $\pm\pi$ kinks in the azimuthal direction (Fig. 1(a)), which increase the frequency to $k_{21}^c = 3.0542/a$ higher than the (1,1) mode where the π kink running along a diameter (Fig. 7(a)) equivalent to a pair of $\pm\pi$ kinks in the azimuthal direction.

The magnetic field penetrates into the cylinder along two directions (Fig. 2(d)), $\phi = 3\pi/4$ and $\phi = -\pi/4$, and flows away along the two orthogonal directions, $\phi = \pi/4$

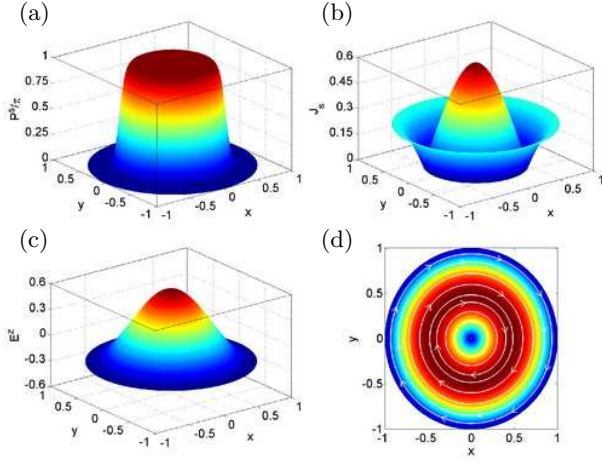


FIG. 3: (color online). Same as Fig. 1 for the (0,1) mode of a cylindrical mesa.

and $\phi = -3\pi/4$, where the absolute value of magnetic field assumes its maximum. The electric field and the supercurrent become maximal at the directions of multiples of $\phi = \pi$'s. The (2,1) mode for the cylinder geometry corresponds to the (1,1) mode for the rectangle geometry [31].

C. (0,1) mode for cylindrical mesa

For comparison, we display in Fig. 3 the patterns for the (0,1) mode for cylinder geometry which has been discussed in Ref. [31]. Since this mode given by

$$P_l(\mathbf{r}, t) = \omega t + AJ_0\left(\frac{\chi_{01}^c}{a}\rho\right) \sin(\omega t + \varphi) + f_l P^s(\mathbf{r}), \quad (10)$$

with $\chi_{01}^c = 3.8317$ the first zero of the derivative of $J_0(z)$, is uniform azimuthally, the π phase kink has to be compressed into the radial direction (Fig. 3(a)). This makes the spatial variation of the magnetic field steep (Fig. 3(d)), and thus the wave number increases to $k_{01}^c = 3.8317/a$, which is to be excited at a voltage higher than the above (1,1) and (2,1) modes. The magnetic field is circular in this mode (Fig. 3(d)), and in order to match the boundary condition at the edge it is suppressed to zero totally. The magnetic field is also suppressed to zero at the center.

D. (1,2) mode for cylindrical mesa

The π phase kink can occur simultaneously in both azimuthal and radial directions. The lowest mode is the (1,2) mode as shown in Fig. 4 given by

$$P_l(\mathbf{r}, t) = \omega t + AJ_1\left(\frac{\chi_{12}^c}{a}\rho\right) \cos \phi \sin(\omega t + \varphi) + f_l P^s(\mathbf{r}), \quad (11)$$

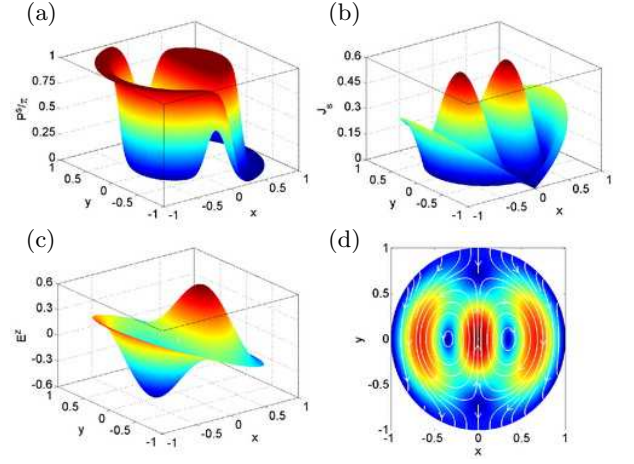


FIG. 4: (color online). Same as Fig. 1 for the (1,2) mode of a cylindrical mesa.

with $\chi_{12}^c = 5.3314$ the second zero of derivative of $J_1(z)$.

E. IV characteristics for cylindrical mesa

The IV characteristics associated with a cavity mode denoted by the eigenfunction $g(\mathbf{r})$ is well approximated by [30, 31, 32, 33]

$$J_{\text{ext}} = \beta\omega \left[1 + \frac{\left(\int_{\Omega} d\mathbf{r} g(\mathbf{r}) \cos P^s \right)^2}{2\Omega \int_{\Omega} d\mathbf{r} (g(\mathbf{r}))^2} \frac{1}{(\omega^2 - k^2)^2 + (\beta\omega)^2} \right], \quad (12)$$

with k the cavity frequency and Ω the cross section of mesa perpendicular to the c axis. The prefactor of the

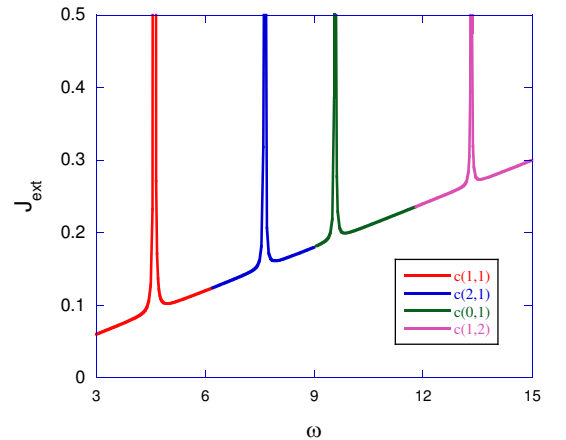


FIG. 5: (color online). IV characteristics for the cylindrical mesa including the four lowest modes. The dimensionless voltage, equal to the wave number and frequency, is given by $\omega = \chi^c/a$ with $\chi^c = 1.8412, 3.0542, 3.8317$ and 5.3314 for the (1,1), (2,1), (0,1) and (1,2) mode, respectively. The radius of cylinder is $a = 0.4$ ($a = 0.4\lambda_c$).

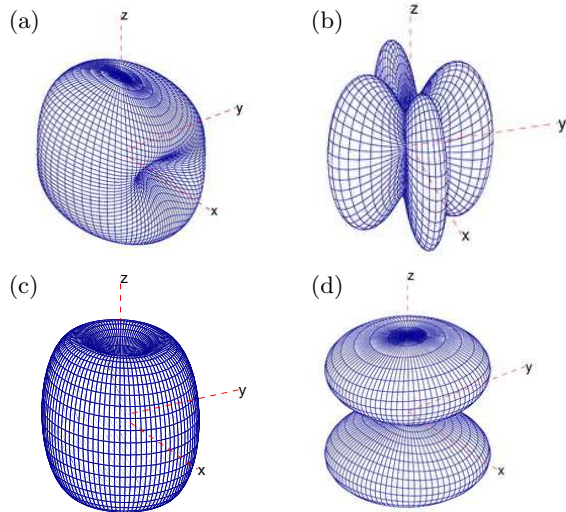


FIG. 6: (color online). Radiation patterns for (a) (1,1) mode, (b) (2,1) mode, (c) (0,1) mode, and (d) (1,2) mode of cylindrical mesa at the respective resonance frequency. The radius of the mesa is $a = 0.4$.

nonlinear resonating term is 0.379, 0.345, 0.357 and 0.314 for the (1,1), (2,1), (0,1) and (1,2) modes, respectively. In Fig. 5, we display the IV characteristics for a cylinder with the radius $a = 0.4$. A treatment with improvement on the peak value of current at the resonance [31] is also available for the present cylindrical geometry.

F. Radiation pattern for cylindrical mesa

The radiation pattern of each mode can be computed by using the Huygens principle [33], and the result is displayed in Fig. 6.

IV. ANNULAR MESA

One of the hurdles for the present technique to excite EM waves of even higher frequency is the heating effect, since the corresponding higher dc voltage injects large currents into the sample resulting in severe Joule heating. One way to overcome this effect may be to dig a hole in the superconductor mesa, rendering for example a cylindrical one to annular, which reduces the cross section, and thus the total current and Joule heating. The inner surface of an annular mesa may help leaking heat generated in the mesa additionally. Tailoring the shape of superconductor mesa however will affect the cavity mode, and thus the radiation frequency in a nontrivial way. In order to check this effect, we need to understand the cavity phenomenon for the annular geometry.

A. (1,1) mode for annular mesa

The (1,1) mode in an annular mesa is given by

$$P_l(\mathbf{r}, t) = \omega t + \left(A_J J_1\left(\frac{\chi_{11}^a}{a_o} \rho\right) + A_N N_1\left(\frac{\chi_{11}^a}{a_o} \rho\right) \right) \cos \phi \sin(\omega t + \varphi) + f_l P^s(\rho), \quad (13)$$

where $N_1(z)$ is the Bessel function of second kind, and $a_o(a_i)$ the outer(inner) radius. The Neumann boundary condition should be satisfied at both the outer and inner surfaces, which determines the coefficient χ_{11}^a for a given radius ratio a_i/a_o :

$$J_1'(\chi_{11}^a \frac{a_i}{a_o}) N_1'(\chi_{11}^a) - J_1'(\chi_{11}^a) N_1'(\chi_{11}^a \frac{a_i}{a_o}) = 0, \quad (14)$$

where $J_1'(z)$ and $N_1'(z)$ are the first derivatives, and the wave number, or equivalently the frequency, is given by $k_{11}^a = \chi_{11}^a/a_o$. The ratio of the coefficients is then determined by

$$A_N/A_J = -J_1'(\chi_{11}^a)/N_1'(\chi_{11}^a). \quad (15)$$

The distributions of the static phase kink, supercurrent, the spatial part of the oscillating electric and magnetic field are displayed in Fig. 7 for the case of $a_i/a_o = 1/2$, with $k_{11}^a = \chi_{11}^a/a_o = 1.3546/a_o$ from Eq. (14).

B. (2,1) mode for annular mesa

The plasma term for (2,1) mode is given by

$$\tilde{P}(\mathbf{r}, t) = \left(A_J J_2\left(\frac{\chi_{21}^a}{a_o} \rho\right) + A_N N_2\left(\frac{\chi_{21}^a}{a_o} \rho\right) \right) \cos(2\phi) \sin(\omega t + \varphi). \quad (16)$$

The wave number of this mode is determined by an equation same to Eq. (14) except for using $J_2'(z)$ and $N_2'(z)$

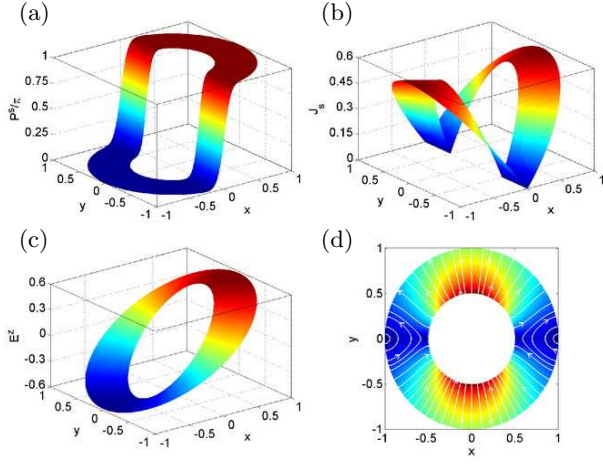


FIG. 7: (color online). Same as Fig. 1 for the (1,1) mode of an annular mesa, except that the lateral coordinates are normalized by the outer radius and the ratio between the inner and outer radii is 1/2.

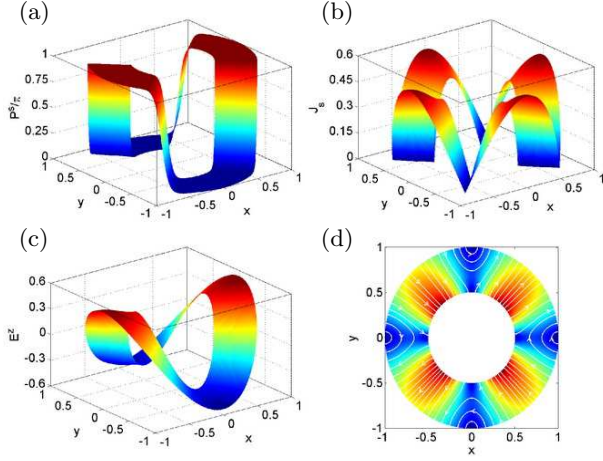


FIG. 8: (color online). Same as Fig. 7 for the (2,1) mode of an annular mesa.

instead of $J_1^a(z)$ and $N_1^a(z)$ as $k_{21}^a = \chi_{21}^a/a_o = 2.6812/a_o$ for $a_i/a_o = 1/2$. The distributions of the static phase kink, supercurrent, the spatial part of the oscillating electric and magnetic field are displayed in Fig. 8, which is to be compared with Fig. 2. Similar to (1,1) mode, the magnetic field becomes along the radial direction in most part of the mesa.

C. (0,1) mode for annular mesa

The plasma term for the (0,1) mode is

$$\tilde{P}(\mathbf{r}, t) = \left(A_J J_0\left(\frac{\chi_{01}^a}{a_o} \rho\right) + A_N N_0\left(\frac{\chi_{01}^a}{a_o} \rho\right) \right) \sin(\omega t + \varphi). \quad (17)$$

The wave number is $k_{01}^a = \chi_{01}^a/a_o = 6.3932/a_o$ for $a_i/a_o = 1/2$. The distributions of the static phase kink,

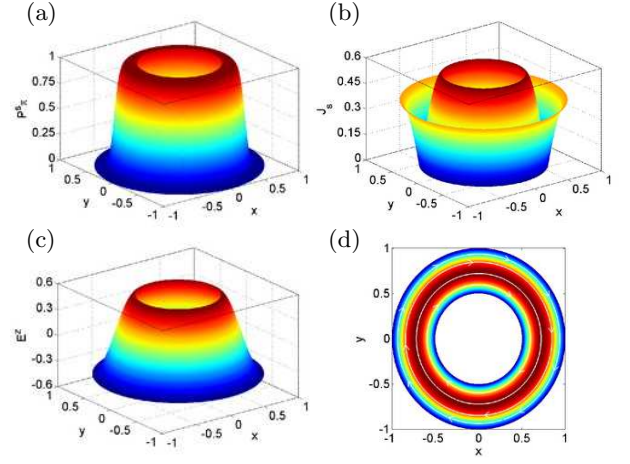


FIG. 9: (color online). Same as Fig. 7 for the (0,1) mode of an annular mesa.

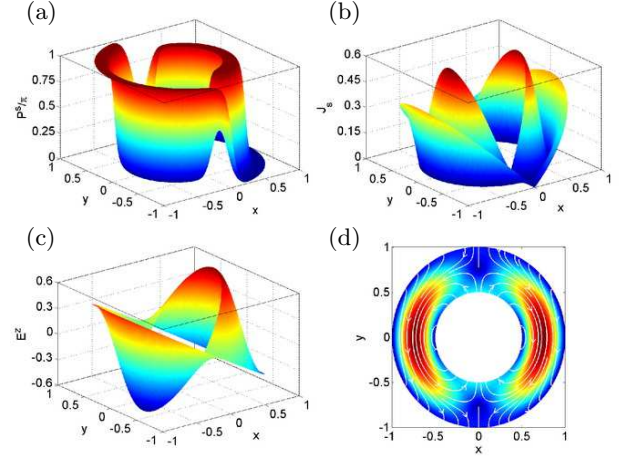


FIG. 10: (color online). Same as Fig. 7 for the (1,2) mode of an annular mesa.

supercurrent, the spatial part of the oscillating electric and magnetic field are displayed in Fig. 9.

In contrast to the modes (1,1) and (2,1), the magnetic field is circular in the (0,1) mode. The system arranges the magnetic field to zero totally at the two surfaces to satisfy the Neumann boundary condition. Thus, the density of magnetic flux increases when the center of cylinder is removed, which results in a higher frequency.

D. (1,2) mode for annular mesa

The plasma term for the (1,2) mode is

$$\tilde{P}(\mathbf{r}, t) = \left(A_J J_1\left(\frac{\chi_{12}^a}{a_o} \rho\right) + A_N N_1\left(\frac{\chi_{12}^a}{a_o} \rho\right) \right) \cos \phi \sin(\omega t + \varphi). \quad (18)$$

The wave number is $k_{12}^a = \chi_{12}^a/a_o = 6.5649/a_o$ for $a_i/a_o = 1/2$. The distributions of the static phase kink,

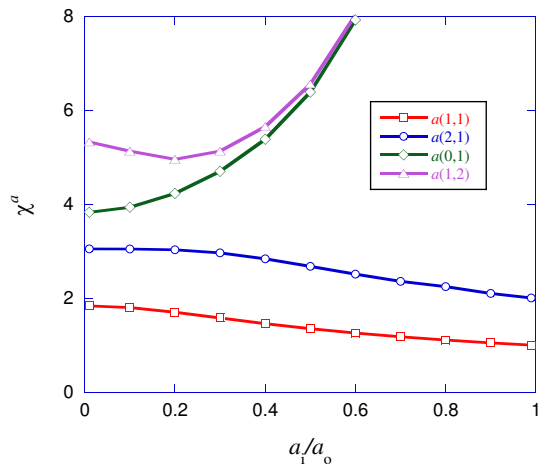


FIG. 11: (color online). Wave-number factor χ^a as a function of the radius ratio a_i/a_o for the lowest four modes for the annular geometry, with the wave number given by $k^a = \chi^a/a_o$.

supercurrent, the spatial part of the oscillating electric and magnetic field are displayed in Fig. 10.

There are two features in the redistribution of magnetic field for this mode as displayed in Fig. 10(d). The maximum of magnetic field at the center of the cylindrical mesa disappears (Fig. 4(d)), similar to (1,1) mode. On the other hand, the density of magnetic flux increases at the other two maxima of magnetic field, similar to (0,1) mode.

E. Dependence of frequency on aspect ratio

The dependence of wave number, and equivalently frequency, on the aspect ratio a_i/a_o is shown in Fig. 11. For the (1,1) and (2,1) modes, the wave number $k^a = \chi^a/a_o$ decreases with increasing ratio a_i/a_o , whereas an opposite trend is seen for the (0,1) mode. The behavior of the (1,2) mode is a compromise of the both trends, yielding a minimum in wave number at $a_i/a_o \simeq 0.2$. These behaviors are well understood from the redistribution of magnetic field in the corresponding cavity modes discussed above.

For the (1,2) mode, the regime $0 \leq a_i/a_o \leq 0.4$ can be used to suppress the Joule heating without changing much the radiation frequency. Since the curves for the (1,1) and (2,1) modes in Fig. 11 are quite flat, they can also be useful for the same purpose. The mode (0,1) and the mode (1,2) with $a_i/a_o > 0.4$ can be used to increase the radiation frequency provided the heating effect can be controlled.

F. IV characteristics for annular mesa

The IV characteristics for the annular mesa is also given by Eq. (12). The prefactor for the (1,1), (2,1),

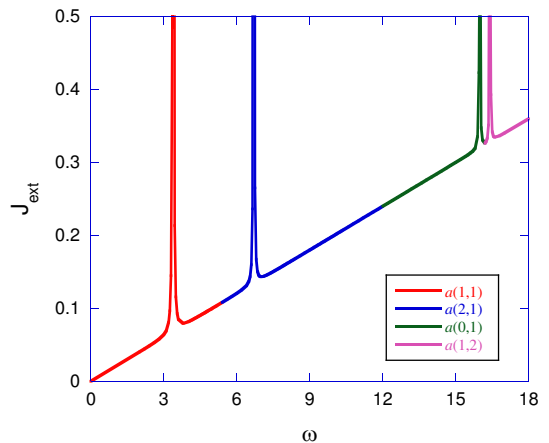


FIG. 12: (color online). IV characteristics for the annular mesa including the four lowest modes. The dimensionless voltage is $\omega = \chi^a/a$ with $\chi^a = 1.3546, 2.6812, 6.3932$ and 6.5649 for the (1,1), (2,1), (0,1) and (1,2) modes respectively. The radii are $a_i = 0.2$ and $a_o = 0.4$.

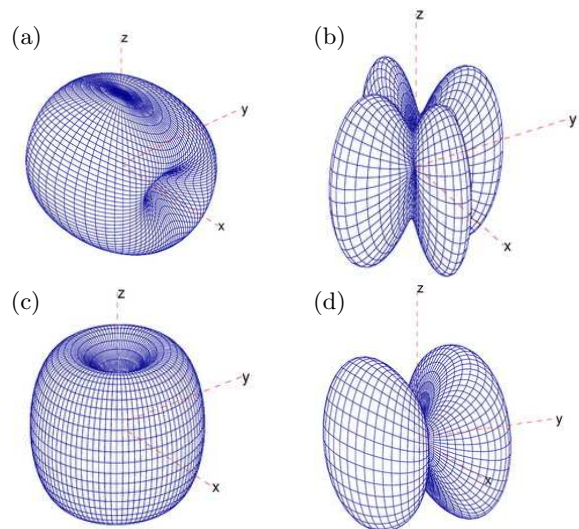


FIG. 13: (color online). Same as Fig. 6 for annular mesa. Multi reflections due to the inner surface are neglected since the thickness of annular mesa is very small compared with the EM wavelength. The radii are $a_i = 0.2$ and $a_o = 0.4$.

(0,1) and (1,2) mode is 0.405, 0.403, 0.396 and 0.321, respectively. The IV characteristics for the annular mesa is displayed in Fig. 12.

G. Radiation pattern for annular mesa

The radiation pattern of each mode is displayed in Fig. 13 for the annular geometry, where multi reflections at the inner radius have been neglected since the mesa thickness is very small compared with the EM wavelength.

V. SUMMARY AND PERSPECTIVES

We first address that the radius dependence of radiation frequency observed in a recent experiment using a cylindrical mesa [34] is to be understood as a clear indication of the right boundary condition for mesa of small thickness compared with the EM wavelength, with which the static π kink state has been derived uniquely for inductively coupled Josephson junctions. Detailed spatial distributions of the superconductivity phase difference with a π phase kink are presented for various cavity modes of cylindrical mesa. Along with them, we also summarize the spatial distribution of the EM standing waves inside the junctions which hopefully can be observed in experiments.

We propose to use annular mesas to excite THz EM radiations. The obvious advantage of the annular geometry is the reduction of heating, since the area of sample is reduced which suppresses the total Joule heating and the inner surface of the sample may enhance heat leakage additionally. The effect of removing the central part of a cylindrical mesa, thus rendering an annular one, on the redistribution of the superconductivity phase difference, the supercurrent and the EM waves is analyzed. It is shown that, depending on the mode, the radiation

frequency varies with the aspect ratio in different ways, and there is plenty of room for modification of the EM radiation by tailoring the shape of sample, while keeping low heating.

Superconductor samples of annular geometry can also be manufactured as a waveguide resonator, where fragments of superconductor mesas are arranged in a thread with each satisfying the condition of small thickness compared with the wavelength of electromagnetic wave. In contrast with the fiber lasers developed for visible lights (see for example [41]), the lasing mode propagates along the annular superconductor, whereas the electromagnetic waves within the inner surface establishes the coherent oscillation in thread of superconductor mesas. When the outer surface is shielded by wrapping a jacket made of appropriate materials, the wave propagating in the waveguide can be enhanced.

VI. ACKNOWLEDGEMENTS

This work was supported by WPI Initiative on Materials Nanoarchitectonics, MEXT of Japan and by CREST, JST of Japan, and partially by ITSNEP of CAS.

-
- [1] B. D. Josephson, *Phys. Lett.* **1**, 251 (1962).
 - [2] A. Barone and G. Paterno, *Physics and Applications of the Josephson Effect*, John Wiley & Sons (1982).
 - [3] I. K. Yanson, V. M. Svistunov, and I. M. Dmitrenko, *Zh. Eksp. Teor. Fiz.* **48**, 976 (1965).
 - [4] A. H. Dayem and C. C. Grimes, *Appl. Phys. Lett.* **9**, 47 (1966).
 - [5] J. E. Zimmerman, J. A. Cowen, and A. H. Silver, *Appl. Phys. Lett.* **9**, 353 (1966).
 - [6] N. F. Pedersen, O. H. Soerensen, J. Mygind, P. E. Lindelof, M. T. Levinsen, and T. D. Clark, *Appl. Phys. Lett.* **28**, 562 (1976).
 - [7] T. F. Finnegan and S. Wahlsten, *Appl. Phys. Lett.* **21**, 541 (1972).
 - [8] A. K. Jain, K. K. Likharev, J. E. Lukens, and J. E. Sauvageau, *Phys. Rep.* **109**, 309 (1984).
 - [9] M. Darula, T. Doderer and S. Beuven, *Supercond. Sci. Technol.* **12**, R1 (1999).
 - [10] P. Barbara, A. B. Cawthorne, S. V. Shitov, and C. J. Lobb, *Phys. Rev. Lett.* **82**, 1963 (1999).
 - [11] R. Kleiner, F. Steinmeyer, G. Kunkel, and P. Müller, *Phys. Rev. Lett.* **68**, 2394 (1992).
 - [12] S. Sakai, P. Bodin, and N. F. Pedersen, *J. Appl. Phys.* **73**, 2411 (1993).
 - [13] M. Tachiki, T. Koyama, and S. Takahashi, *Phys. Rev. B* **50**, 7065 (1994).
 - [14] T. Koyama and M. Tachiki, *Solid State Commun.* **96**, 367 (1995).
 - [15] S. E. Shafranjuk and M. Tachiki, *Phys. Rev. B* **59**, 14087 (1999).
 - [16] E. Kume, I. Iguchi, and H. Takahashi, *Appl. Phys. Lett.* **75**, 2809 (1999).
 - [17] R. Kleiner, T. Gaber, and G. Hechtfisher, *Phys. Rev. B* **62**, 4086 (2000).
 - [18] I. Iguchi, K. Lee, E. Kume, T. Ishibashi, K. Sato, *Phys. Rev. B* **61**, 689 (2000); K. Lee, W. Wang, I. Iguchi, M. Tachiki, K. Hirata, and T. Mochiku, *Phys. Rev. B* **61**, 3616 (2000); I. Iguchi, E. Kume, and H. Takahashi, *Phys. Rev. B* **62**, 5370 (2000).
 - [19] I. E. Batov, X. Y. Jin, S. V. Shitov, Y. Koval, P. Müller, A. V. Ustinov, *Appl. Phys. Lett.* **88**, 262504 (2006).
 - [20] L. N. Bulaevskii and A. E. Koshelev, *Phys. Rev. Lett.* **97**, 267001 (2006).
 - [21] L. N. Bulaevskii and A. E. Koshelev, *J. of Supercond. Novel Magn.* **19**, 349 (2006).
 - [22] L. N. Bulaevskii and A. E. Koshelev, *Phys. Rev. Lett.* **99**, 057002 (2007).
 - [23] M. -H. Bae, H. -J. Lee, and J. -H. Choi, *Phys. Rev. Lett.* **98**, 027002 (2007).
 - [24] A. E. Koshelev and L. N. Bulaevskii, *Phys. Rev. B* **77**, 014530 (2008).
 - [25] S. -Z. Lin, X. Hu, and M. Tachiki, *Phys. Rev. B* **77**, 014507 (2008).
 - [26] B. Ferguson and X. -C. Zhang, *Nat. Mater.* **1**, 26 (2002).
 - [27] M. Tonouchi, *Nat. Photon.* **1**, 97 (2007).
 - [28] L. Ozyuzer, A. E. Koshelev, C. Kurter, N. Gopalsami, Q. Li, M. Tachiki, K. Kadowaki, T. Yamamoto, H. Minami, H. Yamaguchi, M. Tachiki, K. E. Gray, W. -K. Kwok, and U. Welp, *Science* **318**, 1291 (2007).
 - [29] D. N. Langenberg, D. J. Scalapino, B. N. Taylor, and R. E. Eck, *Phys. Rev. Lett.* **15**, 294 (1965).
 - [30] S. -Z. Lin and X. Hu, *Phys. Rev. Lett.* **100**, 247006 (2008).
 - [31] X. Hu and S. -Z. Lin, *Phys. Rev. B* **78**, 134510 (2008).

- [32] A. E. Koshelev, Phys. Rev. B **78**, 174509 (2008).
- [33] S. -Z. Lin and X. Hu, Phys. Rev. B **79**, 104507 (2009).
- [34] K. Kadowaki *et al.*, private communications; in preparation for submission.
- [35] H. -B. Wang, S. Guénon, J. Yuan, A. Iishi, S. Arizawa, T. Hatano, T. Yamashita, D. Koelle, and R. Kleiner, Phys. Rev. Lett. **102**, 017006 (2009).
- [36] K. Kadowaki, H. Yamaguchi, K. Kawamata, T. Yamamoto, H. Minami, I. Kakeya, U. Welp, L. Ozyuzer, A. E. Koshelev, C. Kurter, K. E. Gray and W. -K. Kwok, Physica C **468**, 634 (2008).
- [37] M. Tachiki, S. Fukuya and T. Koyama, arXiv:0810.5268 (to appear in Phys. Rev. Lett. (2009)).
- [38] H. Matsumoto, T. Koyama and M. Machida, Physica C **468**, 654 (2008).
- [39] In most literatures, the first zero the derivative of Bessel function $J_0(z)$ is put as 3.8317. The better description is to put 0 as the first zero and 3.8317 as the second, and so on so forth. The mode shown in Fig. 3 (see also Ref.[31]) would then be assigned as the (0,2) mode in cylinder. The redefined mode (0,1) is the uniform solution, which is not a real cavity mode [33].
- [40] K. Kadowaki *et al.*, preprint.
- [41] Hamamatsu Photonics K. K. Laser Group, Nature Photonics, Sample Issue, 14 (2006).